Int. J. Heat Mass Transfer. Vol. 33. No. 5, pp. 797–803, 1990
Printed in Great Britain

0017–9310/90 $3.00+0.00
© 1990 Pergamon Press plc

Heat transfer in thin silicon film melting by laser line sources

COSTAS P. GRIGOROPOULOS, ASHLEY F. EMERY and EVAN P. WIPF
Department of Mechanical Engineering, FU-10, University of Washington, Seattle, WA 98195, U.S.A.

(*Received* 16 *December* 1988 *and in final form* 12 *June* 1989)

Abstract—Optical melting and recrystallization of thin semiconductor films on amorphous insulators is of importance to semiconductor technology since it can lead to the development of high speed electronic devices. The degree of improvement is affected by the rates of melting and recrystallization. To control these aspects, it is necessary to analyze the heat transfer in both the silicon layer and the insulating substrate. This paper describes numerical predictions based upon an enthalpy approach. The numerical predictions are compared to a limited set of experimental data.

1. INTRODUCTION

RECRYSTALLIZATION of thin semiconductor films which are deposited on amorphous substrates often yields improved electrical and crystalline properties. The recrystallization can be effected by shining a laser source through the substrate (Fig. 1(a)) to melt the semiconductor. The specimen is translated and the material recrystallizes in the wake of the molten spot. To understand the melting process induced by CW argon ion lasers, experiments were performed [1]. These experiments studied the effects of the total power and shape of intensity distribution of the laser beam, as well as of the speed of the translating specimen, on the induced phase change process. The laser beam dimensions were varied by adjusting a focusing lens system to obtain laser beam cross-sectional shapes, which ranged from nearly circular to narrow elliptical profiles. The parameters chosen to quantify the laser beam size are the distances of the points where the laser beam irradiance intensity drops to $1/e$ of its peak intensity from the laser beam center along the beam axes. These distances along the x- and z-axes are denoted by r_x and r_z, respectively, and are indicated in Fig. 1(b), which also shows the respective molten pool dimensions s_x and s_z. Figure 2 shows a typical micrograph of light transmitted through a 0.5 μm thick polysilicon layer during melting using a laser beam of elliptical shape.

Upon examining the experimental results (i.e. Fig. 2), as typified by the geometry of the melt zone, one notices that for laser beams which are elliptical in shape with $r_z > 4r_x$ the edge of the molten zone is nearly parallel to the z-axis over a substantial portion of the pool. Curvature of the leading and trailing fronts becomes noticeable only near the ends of the pool. This argument is supported by the results of three-dimensional conductive heat transfer calculations. Hence, some of the basic characteristics of the process can be determined by considering infinitely wide laser beams, with a laser beam intensity which is a function of x only and which generates straight phase boundaries. Because of the thinness of the silicon layer, the temperature field can be further approximated as one-dimensional in the silicon layer. However, the temperature field must be treated as two-dimensional in the glass substrate. Although this model eliminates the transverse heat conduction in the z-direction, it does include the radiant characteristics of the thin film (absorption and transmission) and the effects of radiation and convection to the ambient surroundings from the sample top and bottom surfaces. The use of such a simple geometry is

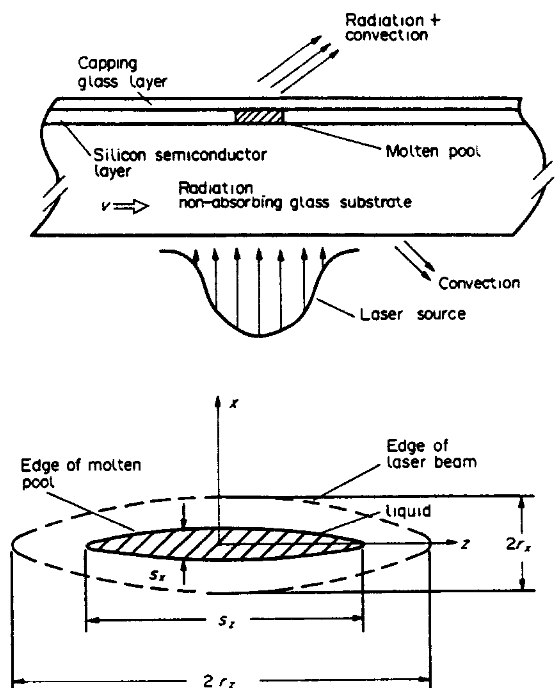

FIG. 1. Schematic showing the relevant dimensions of the molten pool and the laser beam.

NOMENCLATURE

- a absorption coefficient
- c_p specific heat
- d_{si} semiconductor layer thickness
- d_{ss} substrate thickness
- F blackbody radiation factor
- f_l liquid silicon volume fraction
- f_s solid silicon volume fraction
- h_l heat transfer coefficient at the bottom substrate surface
- h_u heat transfer coefficient at the top silicon surface
- H enthalpy
- j imaginary unit
- k thermal conductivity
- L latent heat of fusion
- $\hat{n}_l$ liquid silicon complex refractive index
- P laser beam total power
- Q_{ab} heat absorbed by the thin silicon layer
- Q_{ext} external laser light source irradiance distribution
- Q_0 peak power intensity of a laser line source having a uniform distribution in the normal to the motion direction
- Q_0^* reference laser beam peak intensity
- Q_{rad} radiation loss from the silicon layer through the capping layer and the glass substrate
- R thin film reflectivity
- R_n normal incidence reflectance
- r_x distance along the x-axis from the laser beam center where the laser beam irradiance intensity drops to $1/e$ of its peak value (Fig. 1(b))
- r_z distance along the z-axis from the laser beam center where the laser beam irradiance intensity drops to $1/e$ of its peak value (Fig. 1(b))
- s_x molten pool size along the x-direction (Fig. 1(b))
- s_z molten pool size along the normal to the motion direction (Fig. 1(b))
- t time
- T temperature
- T_m melting temperature
- T_∞ ambient temperature
- V material translation speed
- x coordinate in the scanning direction
- x_m distance of the melting front from the laser beam center (Fig. 3)
- x_s distance of the solidification trailing edge from the laser beam center (Fig. 3)
- y coordinate normal to the sample surface
- z coordinate in the transverse direction.

Subscripts

- l liquid silicon
- s solid silicon
- si silicon
- ss substrate.

Greek symbols

- ε emissivity
- λ laser light wavelength
- ρ density
- σ Stefan–Boltzmann constant
- τ thin film transmissivity.

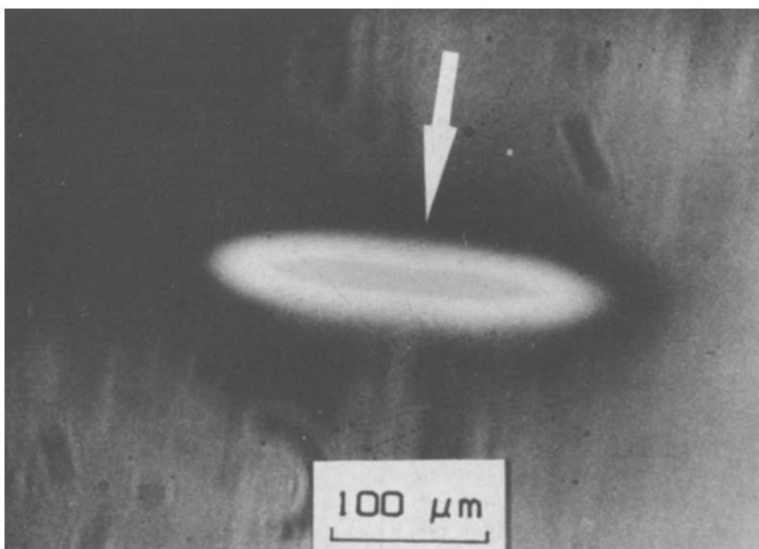

FIG. 2. A micrograph of light transmitted through a 0.5 μm thick polysilicon layer during melting. An argon ion laser beam of elliptical cross-sectional shape, $P = 1.3$ W, $r_x = 17$ μm, $r_z = 93$ μm is used. The sample is translated in the direction of the arrow, with a speed, $V = 2$ mm s^{-1}. The opaque molten silicon pool is surrounded by bright, hot solid silicon.

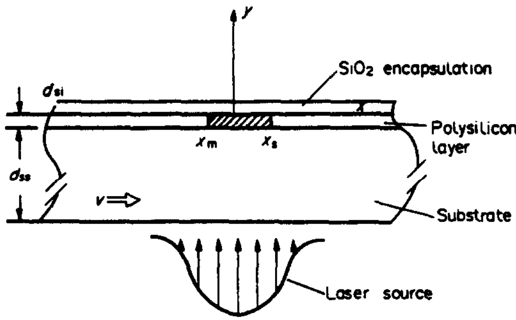

FIG. 3. Cross section through a 0.5 μm thick polysilicon layer deposited on a glass substrate of 0.5 mm thickness and encapsulated by a 0.5 μm thick glass layer. The layer is being irradiated by a laser beam that propagates through the transparent glass substrate.

justified on the basis that both the circular and the highly elliptical laser beam driven melt zones exhibit the same basic behavior with regard to variations in the translation speed [1].

The steady-state temperature distribution for melting of a silicon slab by a stationary laser light source was given in ref. [2]. The enthalpy formulation of phase change problems, along with simplifying assumptions was used in ref. [3] to obtain the transient temperature distribution for a thick silicon slab irradiated by a stationary light source. The temperature transients for thin film melting with scanning incoherent light sources of uniform intensity distribution in the transverse to the scanning direction ($r_z = \infty$) were obtained in ref. [4]. This analysis used a piecewise linear function to approximate the temperature–enthalpy relation and Kirchhoff's transformation to relax the temperature dependence of the material properties. An approximate solution for the temperature field transients in the melting of thin silicon layers with scanning laser beams of elliptical or circular symmetry was given in ref. [5]. One-dimensional finite difference models were employed in ref. [6] to study the effects of the light beam scan rate and of the capping layer structure on the power threshold for thin film melting.

Analytical conductive heat transfer models for the steady-state temperature distribution in thin silicon films irradiated by laser beams of constant cross section in the normal to the motion direction were given in refs. [7, 8]. A semiempirical model for the calculation of the dimensions of the molten pool induced by scanning laser beams was given in ref. [9].

It is the intent of this paper to construct a numerical model that will generate results for comparison with the experimental data. A finite difference representation, based on the enthalpy formulation [10–12] will be used. This approach was adopted in ref. [13] in three-dimensional numerical simulations of radiative thin film silicon melting.

2. ANALYSIS

A sketch of the basic structure is shown in Fig. 3. A 0.5 μm thick polysilicon layer is deposited on a 0.5 mm thick glass substrate. The silicon layer is encapsulated by a 0.5 μm thick glass layer that prevents surface tension driven mass transport that would otherwise occur due to the extremely high temperature gradients involved. The argon laser beam ($\lambda = 0.5145$ μm) passes through the transparent and non-radiatively participating for visible wavelengths substrate and is then partially absorbed by the polysilicon layer. The molten pool dimension in the direction of motion is defined to be $s_x = x_s - x_m$. Since both the capping material and the semiconductor are very thin (each 0.5 μm), the temperature variation across the thickness can be ignored. The cap and the polysilicon film are henceforth collectively referred to as the 'silicon layer' the properties (capacitance, conductivity, transmissivity, etc.) of which are specified so as to account for the relative amounts of both. The temperature is thus specified by the function, $T_{si}(x, t)$. On the other hand, the substrate is relatively thick and poorly conducting and its temperature field is two-dimensional. The temperature histories, $T_{si}(x, t)$ and $T_{ss}(x, y, t)$ are computed by considering a Cartesian coordinate system attached to the center of the laser beam (Fig. 3). For temperatures below the melting temperature, the heat transfer in the solid silicon layer is represented by the heat conduction equation integrated across its thickness

$$\rho_{si}(T_{si})C_{p,si}(T_{si})\left(\frac{\partial T_{si}}{\partial t}+V\frac{\partial T_{si}}{\partial x}\right)=\frac{\partial}{\partial x}\left(k_{si}(T_{si})\frac{\partial T_{si}}{\partial x}\right)$$

$$+\frac{Q_{ab}(x,t,T_{si})-Q_{rad}(T_{si})-h_u(T_{si}-T_\infty)-k_{si}(T_{si})\left.\frac{\partial T_{si}}{\partial y}\right|_{y=-d_{ss}}}{d_{si}}. \quad (1)$$

The term $h_u(T_{si}-T_\infty)$ represents the energy convected from the silicon layer surface to the ambient atmosphere. The coefficient h_u is an effective coefficient which is found by combining the convective resistance at the surface with the thermal resistance of the capping material. The laser beam energy which passes through the transparent substrate and is absorbed by the silicon layer, Q_{ab}, is given by

$$Q_{ab}(x, T_{si}) = [1-R(T_{si})-\tau(T_{si})]Q_{ext}(x). \quad (2a)$$

Glass is virtually transparent up to $\lambda = 4$ μm. For this wavelength the extinction coefficient is 5.79×10^{-5} [14]. Absorption in the capping layer is negligible because of its small thickness. The radiation loss from the surfaces of the silicon layer is

$$Q_{rad} = F_{0\to4\,\mu m}\varepsilon\sigma(T_{si}^4-T_\infty^4). \quad (2b)$$

The intensity of the laser beam, $Q_{ext}(x)$, is assumed to be Gaussian in the direction of translation

$$Q_{ext}(x) = Q_0\exp\left[-\frac{x^2}{r_x^2}\right]. \quad (3)$$

R, τ are the reflectivity and transmissivity of the silicon layer (see Appendix).

The heat conduction equation in the glass substrate is given by

$$\rho_{ss}(T_{ss})c_{p,ss}(T_{ss})\left(\frac{\partial T_{ss}}{\partial t}+V\frac{\partial T_{ss}}{\partial x}\right) = \frac{\partial}{\partial x}\left(k_{ss}(T_{ss})\frac{\partial T_{ss}}{\partial x}\right)+\frac{\partial}{\partial y}\left(k_{ss}(T_{ss})\frac{\partial T_{ss}}{\partial y}\right). \quad (4)$$

Continuity of temperature and heat flux is applied at the interface between the silicon layer and the substrate. Heat is lost by convection and radiation from the upper surface of the silicon layer and by convection from the bottom surface of the substrate. The convective boundary condition at the bottom substrate surface is

$$k_{ss}\frac{\partial T_{ss}}{\partial y}\bigg|_{y=-(d_{si}+d_{ss})} = h_l[T_{ss}(x, -(d_{si}+d_{ss}))-T_\infty]. \quad (5)$$

The enthalpy function, H, is introduced to account for phase changes. Away from the melting temperature, T_m

$$H_{si}(T) = \int_0^T \rho_{si}(T)c_{p,si}(T)\,\mathrm{d}T,\ T<T_m \quad (6a)$$

$$H_{si}(T) = \int_0^T \rho_{si}(T)c_{p,si}(T)\,\mathrm{d}T+L,\ T>T_m \quad (6b)$$

where ρ_{si} and $c_{p,si}$ vary differently with temperature in the solid and liquid phases. For $T=T_m$ the enthalpy function assumes values between $H_{s,si}$ and $H_{l,si}$ where

$$H_{s,si} = \int_0^{T_m} \rho_{si}(T)c_{p,si}(T)\,\mathrm{d}T \quad (6c)$$

$$H_{l,si} = \int_0^{T_m} \rho_{si}(T)c_{p,si}(T)\,\mathrm{d}T+L. \quad (6d)$$

The enthalpy value $H=H_{s,si}$ is assigned to solid material at the melting temperature, while $H=H_{l,si}$ corresponds to pure liquid at the same temperature. Thus, there exists a region in which the melting is partial, and is defined by

$$H_{s,si}<H_{si}<H_{l,si},\ T=T_m. \quad (7)$$

Each point within this region can be assigned a solid fraction $f_s(x,t)$ and a liquid fraction $f_l(x,t)$ for which

$$f_s(x,t)+f_l(x,t) = 1. \quad (8)$$

Thus, the enthalpy function during melting at $T=T_m$, is given by

$$H_{si} = H_{s,si}+f_lL. \quad (9)$$

The enthalpy function in the glass substrate is

$$H_{ss}(T) = \int_0^T \rho_{ss}(T)c_{p,ss}(T)\,\mathrm{d}T. \quad (10)$$

Using the enthalpy as the dependent variable, along with the temperature, equation (1) is written as

$$\frac{\partial H_{si}(T_{si})}{\partial t}+V\frac{\partial H_{si}(T_{si})}{\partial x} = \frac{\partial}{\partial x}\left(k_{si}(T_{si})\frac{\partial T_{si}}{\partial x}\right) + \frac{Q_{ab}(x,t,T_{si})-Q_{rad}(T_{si}) -h_u(T_{si}-T_\infty)-k_{si}(T_{si})\frac{\partial T_{si}}{\partial y}\Big|_{y=-d_{si}}}{d_{si}}. \quad (11)$$

The initial temperature is assumed to be the ambient temperature, T_∞. For short times, when the temperature in the silicon layer is below the melting temperature, the heat conduction equation is solved by a two-step ADI finite difference algorithm. When the temperature in the silicon layer reaches the melting temperature at any location, equation (11) is solved using a Gauss–Seidel iteration scheme for the liquid phase fraction, f_l, and the enthalpy, H_{si}. All the material properties are functions of temperature and melt fraction, although kept constant for each time step.

3. RESULTS

The computational domain was discretized by using an orthogonal mesh of non-uniform grid spacing. In the region of high temperature gradients, a constant grid spacing of 1 μm was applied in the x-direction. The grid spacing in the y-direction was also variable, with the first few points close to the silicon layer placed 0.5 μm apart and subsequent points spaced on increasing distances apart in y. The calculations were carried out for the range of parameters that matches the experimental data. Of particular interest is the quasi-steady temperature distribution, with respect to the fixed system of coordinates. This quasi-steady temperature distribution is established when the initial transient effects vanish.

Figure 4 gives the maximum temperature rise in the silicon layer as a function of time for a laser beam with $Q_0 = 1.95\times10^8$ W m^{-2}, $r_x = 17$ μm and $V=$ 2 mm s^{-1}. These parameters correspond to the micro-

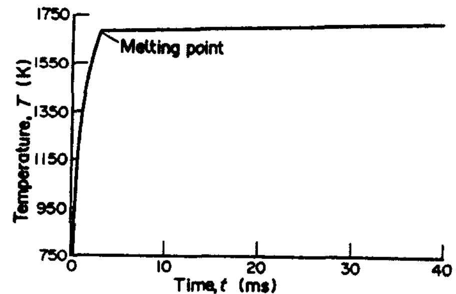

FIG. 4. Maximum temperature rise in the silicon layer as a function of time for a laser beam of $Q_0 = 1.95\times10^8$ W m^{-2}, $r_x = 17$ μm. The material translation speed $V = 2$ mm s^{-1}.

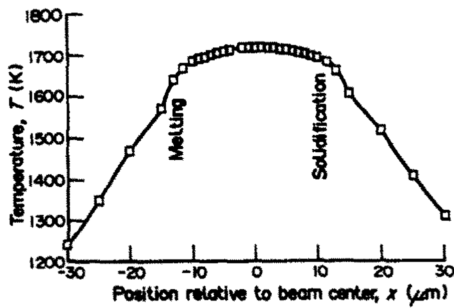

FIG. 5. Temperature distribution in the silicon layer for a laser beam of $Q_0 = 1.95 \times 10^8$ W m^{-2}, $r_x = 17$ μm. The sample translation speed $V = 2$ mm s^{-1}.

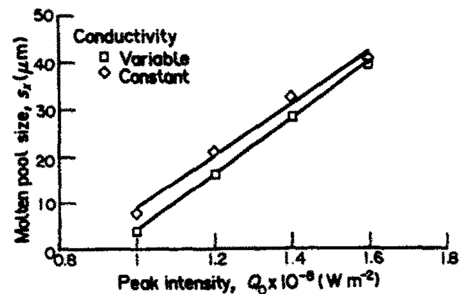

FIG. 7. Effect of temperature variation of the substrate thermal conductivity on the predicted molten pool size for a laser beam of $r_x = 26$ μm and a material translation speed of $V = 2$ mm s^{-1}.

graph shown in Fig. 2. This calculation shows that melting starts after an elapsed time of 3.2 ms and that at $t = 40$ ms, an essentially quasi-steady temperature field has been developed. The quasi-steady temperature distribution in the silicon layer is shown in Fig. 5. The asymmetry introduced by the translational velocity is small and the maximum temperature is only a few tens of Kelvin above the melting temperature of 1685 K. The molten region ($s_x = 20$ μm), is significantly narrower than the laser beam intensity profile ($2r_x = 34$ μm). Figure 6 shows numerical predictions of the molten pool size that were obtained by varying the laser beam dimension, r_x, and the peak intensity, Q_0, and by assuming a constant translation speed, $V = 2$ mm s^{-1}, and a constant substrate thermal conductivity of $k_{ss} = 1.8$ W m^{-1} K^{-1}. Although the temperature dependence of the substrate material thermal conductivity is not well known, it is of interest to determine the importance of the effect when a reasonable variation with temperature is considered. Calculations were made for a substrate material corresponding to a high temperature fused-silica that has the following dependence of thermal conductivity on temperature [15]:

$$k_{ss}(T) = 4.639 \times 10^{-10}\,T^3 - 2.308 \times 10^{-6}\,T^2 + 3.9063 \times 10^{-3}\,T \text{ (W m}^{-1}\text{ K}^{-1}\text{)}. \quad (12)$$

Figure 7 shows the effect of this temperature variation on the numerical prediction of the molten pool size for a laser beam of $r_x = 26$ μm compared with the results obtained for a constant average thermal conductivity of 1.8 W m^{-1} K^{-1}. While there is an increase in the molten pool dimensions due to a variable conductivity, the dependence with respect to the beam intensity, as described by the slope of the curve, does not appear to be significantly changed. A range of constant thermal conductivity from $k_{ss} = 1.4$ to 2.2 W m^{-1} K^{-1} was used to determine the effects of peak beam intensity, Fig. 8. It is clear from Figs. 7 and 8 that the dimension, s_x, of the pool is nearly linearly related to both substrate average conductivity and peak beam intensity. Figure 9 shows the variation of the computed locations of the melting front and of the solidification trailing edge with the laser beam peak intensity, Q_0, for a material translation speed, $V = 2$ mm s^{-1}, and a substrate thermal conductivity, $k_{ss} = 1.8$ W m^{-1} K^{-1}. For this speed, the phase boundary locations are approximately symmetrical over the range of intensities considered.

In general, speeds of the order of 1 mm s^{-1} have been found to be effective in the recrystallization of

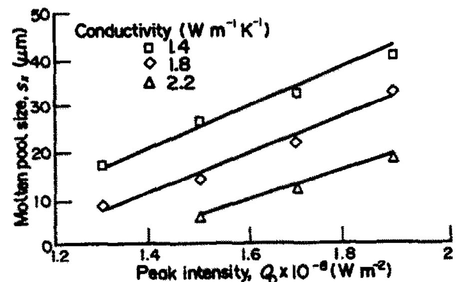

FIG. 8. Effect of substrate thermal conductivity on the molten pool size for a laser beam of $r_x = 19$ μm. The material translation speed $V = 2$ mm s^{-1}.

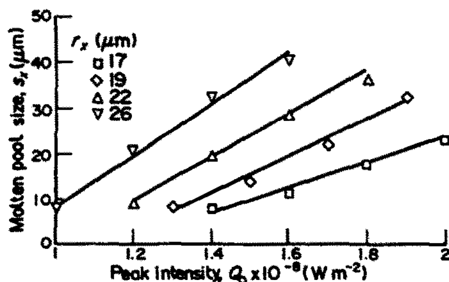

FIG. 6. Numerical predictions of the molten pool dimensions, s_x. The material translation speed $V = 2$ mm s^{-1}.

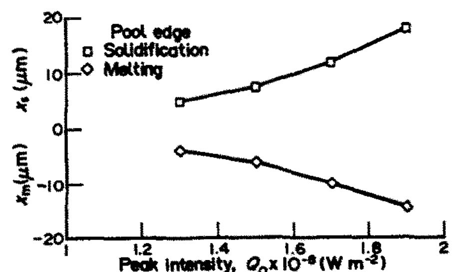

FIG. 9. Computed locations of the solidification edge, x_s, and the melting front, x_m, for $r_x = 19$ μm, $V = 2$ mm s^{-1}.

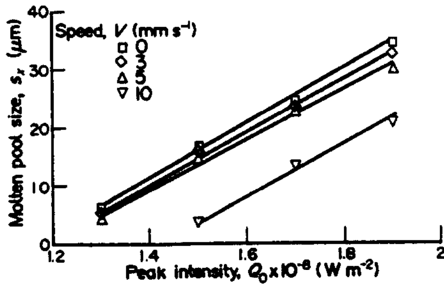

FIG. 10. Effect of material translation speed variation on the molten pool size predictions for a laser beam of $r_x = 19$ μm.

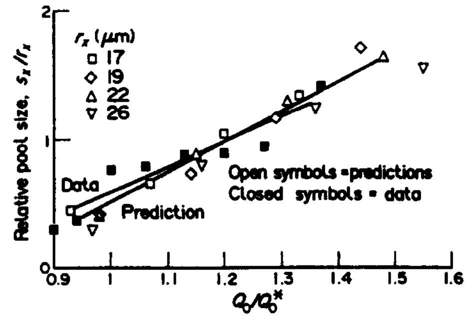

FIG. 12. Plot of the normalized pool dimensions, s_x/r_x, vs the normalized laser beam peak intensities, Q_0/Q_0^*. Q_0^* is the calculated peak irradiance value for a molten pool size $s_x = 10$ μm.

thin silicon films [16, 17]. Figure 10 shows that indeed, speeds of this magnitude have little effect on the molten pool size and geometry. As the material translation speed is increased, the asymmetry in the location of the phase boundaries is enhanced, and higher thermal gradients are applied at the solidification trailing edge with a resulting reduction in the molten pool size. The considerable reduction in pool size for a speed of 10 mm s^{-1} as compared to the nearly constant value for speeds of 3 and 5 mm s^{-1} suggest that speeds should be in the neighborhood of 3 mm s^{-1} to eliminate translation speed effects.

Figure 11 shows the comparison of the numerical calculation with the experimental data given in ref. [1] for laser beams with $r_z > 4r_x$ and a constant material translation speed of $V = 2$ mm s^{-1}. The numerical predictions show the same basic trends as the experimental data. It can be seen that as expected the agreement is better for narrow laser beams of high aspect ratios for which the two-dimensional approximation is more appropriate. As the laser beam becomes more circular, the curvature of the molten pool boundaries increases, the transverse conduction in the z-direction is enhanced, and the agreement deteriorates.

Plotting of a normalized pool size vs a normalized laser beam peak intensity, Q_0/Q_0^*, Fig. 12, yields a nearly straight line relation. The solid lines are the best fit linear regression lines. Differences between the measured and predicted values are felt to be due to errors in treating the radiation lost from the molten pool, temperature dependent thermal and radiative

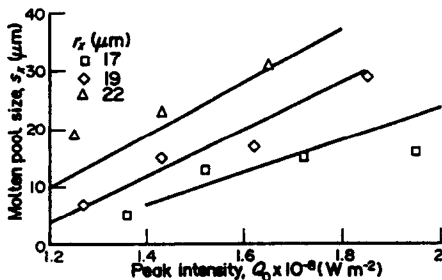

FIG. 11. Molten pool dimensions, s_x, along the direction of motion. The marked points indicate the experimentally measured data. The solid lines give the computed corresponding values for a constant substrate thermal conductivity $k_s = 1.8$ W m^{-1} K^{-1}. The material translation speed $V = 2$ mm s^{-1}.

properties. In spite of these deviations, there is reasonable agreement between the general trends.

The experimental results [1] show that occurrence of partial melting regions, where the solid and the liquid silicon phases coexist, is experimentally observed. This phase coexistence is limited and controlled by liquid–solid surface free energy effects [7], that have not been accounted for in this model. It is therefore not expected that the numerical scheme can analyze the microstructural details that dominate the inhomogeneous melting mechanisms. This microscopic phenomenon can explain the deviation of the numerical predictions from the experimental data for increased beam sizes. For a laser beam of $r_x = 22$ μm, a strong tendency toward partial melting is observed when the beam power density is not sufficient to maintain uniform melting. For a laser beam of $r_x = 26$ μm, melting occurs in the form of a mushy zone, with the fraction of the solid silicon phase increasing for decreasing beam power density.

4. CONCLUSIONS

A simple computational model was constructed for the heat transfer analysis of laser melting of thin silicon films by laser line sources. The effects of the material translation speed and of the laser beam power density were examined. The results showed reasonable agreement with experimental data, thus establishing a framework for analysis. This work has been extended to the full three-dimensional computational analysis of thin film laser melting. Current work is focused on exploring the relation between the computed results and semiconductor laser crystal growth improvements.

Acknowledgement—Support to the first of the authors by NSF, Mechanics, Solids, and Materials Division, under Grant MSM-8708757 is gratefully acknowledged.

REFERENCES

1. C. P. Grigoropoulos, R. H. Buckholz and G. A. Domoto, An experimental study on laser annealing of thin silicon layers, *J. Heat Transfer* **110**, 416–423 (1988).

2. S. A. Kokorowski, G. L. Olson and L. D. Hess, Thermal analysis of CW laser annealing beyond the melt temperature, *Proc. Materials Research Society* (Edited by J. F. Gibbons *et al.*), Vol. 1, pp. 139–146. North-Holland, New York (1981).
3. P. Schvan and R. E. Thomas, Time dependent heat flow calculation of CW laser-induced melting of silicon, *J. Appl. Phys.* **57**(10), 4738–4741 (1985).
4. K. Kubota, C. E. Hunt and J. Frey, Thermal profiles during recrystallization of silicon insulator with scanning incoherent light line sources, *Appl. Phys. Lett.* **46**(12), 1153–1155 (1986).
5. D. Waechter, P. Schvan, R. E. Thomas and N. G. Tarr, Modeling of heat flow in multilayer CW laser-annealed structures, *J. Appl. Phys.* **59**(10), 3371–3374 (1986).
6. I. N. Miaoulis and B. B. Mikic, Heat source power requirements for high-quality recrystallization of thin silicon films for electronic devices, *J. Appl. Phys.* **59**(5), 1658–1666 (1986).
7. C. P. Grigoropoulos, R. H. Buckholz and G. A. Domoto, A thermal instability in the laser-driven melting and recrystallization of thin silicon films on glass substrates, *J. Heat Transfer* **109**, 841–847 (1987).
8. C. P. Grigoropoulos, R. H. Buckholz and G. A. Domoto, An experimental and theoretical study on laser driven phase boundary stability, ASME Paper 87-WA/HT-3 (1987).
9. G. J. Willems, J. J. Poortmans and H. E. Maes, A semi-empirical model for the laser-induced molten zone in the recrystallization process, *J. Appl. Phys.* **62**(8), 3408–3415 (1987).
10. D. R. Atthey, A finite difference scheme for melting problems, *J. Inst. Math. Applic.* **13**, 353–365 (1974).
11. N. Shamsundar and E. M. Sparrow, Analysis of multidimensional conduction phase change via the enthalpy model, *J. Heat Transfer* **97**, 333–340 (1975).
12. N. Shamsundar and E. M. Sparrow, Effect of density change on multidimensional conduction phase change, *J. Heat Transfer* **98**, 551–557 (1977).
13. C. P. Grigoropoulos, R. H. Buckholz and G. A. Domoto, A heat transfer algorithm for the laser-induced melting and recrystallization of thin silicon layers, *J. Appl. Phys.* **60**(7), 2304–2309 (1986).
14. E. D. Palik, *Handbook of Optical Constants of Solids*, p. 760. Academic Press, Orlando (1985).
15. Y. S. Touloukian, *Thermophysical Properties of Matter*. IFI/Plenum, New York (1970).
16. J. C. C. Fan, B. Y. Tsaur and M. W. Geis, Graphite-strip-heater zone-melting recrystallization of Si films, *J. Cryst. Growth* **63**, 453–483 (1983).
17. L. Pfeiffer, A. E. Gelman, K. A. Jackson and K. A. West, Growth mechanisms during thin film crystallization from the melt, *Proc. Materials Research Society* (Edited by M. O. Thompson *et al.*), Vol. 74, pp. 543–553. MRS, Pittsburgh (1987).
18. G. E. Jellison, Jr. and F. A. Modine, Optical functions of silicon between 1.7 and 4.7 eV at elevated temperatures, *Phys. Rev. B* **27**, 7466–7472 (1983).
19. K. M. Shvarev, B. A. Baum and P. V. Gel'd, Optical properties of liquid silicon, *Sov. Phys. Solid State* **16**(11), 2111–2112 (1975).
20. M. Born and E. Wolf, *Principles of Optics* (6th Edn), p. 627. Pergamon Press, Oxford (1970).

APPENDIX

The solid silicon absorption coefficient, a, and the normal incidence reflectance, R_n, for the $\lambda = 514.5$ nm argon ion laser light wavelength have been measured [18]

$$a(T) = 1.24 \exp\left[0.00226(T-300)\right]\ (\mu\mathrm{m}^{-1}) \tag{A1}$$

$$R_n(T) = 0.382 + 5\times 10^{-5}(T-300). \tag{A2}$$

The liquid silicon complex refractive index is [19]

$$\hat{n}_l = 2.2 + j4.4. \tag{A3}$$

The thin film transmissivity and reflectivity are calculated using thin film optics [20]. The silicon thermal conductivity has a significant variation with temperature [15]

$$k_{sf}(T) = 2.99\times 10^4/(T-99)\ (\mathrm{W\ m^{-1}\ K^{-1}}). \tag{A4}$$

The solid silicon volumetric specific heat varies with temperature as follows:

$$\rho_{si}(T)C_{p,si}(T) = 1.45\times 10^6 + 86\,500 \times (T-270)^{0.23}\ (\mathrm{J\ K^{-1}}). \tag{A5}$$

TRANSFERT THERMIQUE DANS UN FILM MINCE DE SILICONE FONDU PAR DES SOURCES LINEAIRES LASER

Résumé—La fusion optique et la recristallisation des films minces semi-conducteurs sur des isolants amorphes est un mécanisme important pour la technologie des semi-conducteurs car il peut conduire au développement d'appareils électroniques à grande vitesse. Le degré d'amélioration est sensible aux vitesses de fusion et de recristallisation. Pour contrôler cela, il est nécessaire d'analyser le transfert thermique à la fois dans la couche de silicone et dans le substrat isolant. On décrit les prédictions numériques basées sur l'approche enthalpique. Les résultats numériques sont comparés à un jeu limité de données expérimentales.

WÄRMETRANSPORT BEIM SCHMELZEN EINES DÜNNEN SILIZIUMFILMS DURCH EINE LINIENFÖRMIGE LASERQUELLE

Zusammenfassung—Der durch Laserbestrahlung ausgelöste Schmelzvorgang und die darauf folgende Rekristallisation einer dünnen Halbleiterschicht auf einem amorphen Isolator ist von großer Bedeutung für die Halbleiter-Technologie, da dies zur Entwicklung von sehr schnell schaltenden elektronischen Bauteilen führen kann. Der Grad der Verbesserung wird durch die Geschwindigkeit der Vorgänge beim Schmelzen und Rekristallisieren beeinflußt. Um diese Vorgänge zu steuern, ist es erforderlich, den Wärmetransport sowohl in der Silizium- als auch der Isolationsschicht zu untersuchen. Es werden numerische Ergebnisse vorgestellt, die mit einem Enthalpiebilanz-Verfahren berechnet worden sind. Diese Ergebnisse werden mit einigen wenigen Meßdaten verglichen.

ТЕПЛОПЕРЕНОС В ТОНКИХ СИЛИКОНОВЫХ ПЛЕНКАХ, РАСПЛАВЛЯЕМЫХ ЛАЗЕРНЫМИ ЛИНЕЙНЫМИ ИСТОЧНИКАМИ

Аннотация—Оптическая плавка и рекристаллизация тонких полупроводниковых пленок на аморфных изоляторах являются важными областями полупроводниковой технологии, т.к. позволяют усовершенствовать высокоскоростные электронные установки. Степень усовершенствования зависит от скорости плавления и рекристаллизации. Для контролирования этих процессов требуется анализ теплопереноса как в силиконовом слое, так и в изоляционной подложке. Описываются численные расчеты, основанные на методе энтальпии. Численные расчеты сравниваются с ограниченным количеством экспериментальных данных.